Atmospheric and Oceanic Science Letters 15 (2022) 100206

Contents lists available at ScienceDirect

Atmospheric and Oceanic Science Letters

journal homepage:
http://www.keaipublishing.com/en/journals/atmospheric-and-oceanic-science-letters/

Distinct patterns of monthly Southern Annular Mode events

Minglin Zheng [a,b], Xiuzhen Li [b,c,*]

[a] College of Meteorology and Oceanography, National University of Defense Technology, Changsha, China
[b] School of Atmospheric Sciences, Sun Yat-sen University, Southern Marine Science and Engineering Guangdong Laboratory (Zhuhai), China
[c] Guangdong Province Key Laboratory for Climate Change and Natural Disaster Studies, Sun Yat-sen University, Zhuhai, China

ARTICLE INFO

Keywords:
Southern Annular Mode
Self-organizing map
Zonal asymmetry
Antarctica
关键词:
南半球环状模
自组织映射网络
纬向不对称性
南极洲

ABSTRACT

The Southern Annular Mode (SAM) is the leading mode of atmospheric variability in the mid–high latitudes of the Southern Hemisphere, representing large-scale variations in pressure and the polar front jet (PFJ). In SAM events, the combination of the SAM and other modes may result in different atmospheric patterns. In this study, a neural-network-based cluster technique, the self-organizing map, was applied to extract the distinct patterns of SAM events on the monthly time scale based on geopotential height anomalies at 500 hPa. Four pairs of distinguishable patterns of positive and negative SAM events were identified, representing the diversity in spatial distribution, especially the zonal symmetry of the center of action at high latitudes—that is, symmetric patterns, split-center patterns, West Antarctica patterns, and a tripole pattern. Although the SAM is well known to be belt-shaped, within the selected SAM events, the occurrence frequency of symmetric patterns is only 23.8%—less than that of West Antarctica patterns. Diverse PFJ variations were found in the symmetric and asymmetric patterns of SAM events. The more asymmetric the spatial distribution of the pressure anomaly, the more localized the adjusted zonal wind anomaly. The adjusted PFJ varied in meridional displacement and strength in different patterns of SAM events. In addition, the entrance and exit of the jet changed in most of the patterns, especially in the asymmetric patterns, which might result in different climate impacts of the SAM.

摘要

南半球环状模 (SAM) 是南半球中–高纬度地区大气变化的主导模态, 表现为气压和极锋急流 (PFJ) 的大尺度变动, 形成强烈的气候影响. 当SAM事件发生时, 气压场异常可呈现出不同的空间结构. 本文利用自组织映射网络方法对月尺度的SAM事件进行分类, 可识别出四对具有显著差异的正, 负SAM事件类型, 包括对称型, 中心分裂型, 西南极洲型和一种三极型分布. 气压异常的空间分布越不对称, 调整后的纬向风异常越局地化. PFJ的经向位移和强度变化入口和出口的变化, 可能导致了SAM的不同气候影响.

1. Introduction

The Southern Annular Mode (SAM) is a large-scale mode of climate variation, spanning the entire extratropical Southern Hemisphere and explaining 25%–30% of the variability of atmospheric mass in the mid and high latitudes (Gong and Wang, 1999; Li, 2015; Fogt and Marshall, 2020). The positive (negative) phase of the SAM is characterized by relatively higher (lower) pressure/geopotential height in the midlatitudes and the opposite appears across the Antarctica (Gong and Wang, 1999). It can form naturally without external forcing, and change via low-frequency processes (Limpasuvan and Hartmann, 2000; Li and Li, 2010, 2012). There is significant surface climate response in the Southern Hemisphere to the SAM, including changes in storm track, wind, temperature, and precipitation (Thompson and Wallace, 2000; Fogt et al., 2012; Gillett et al., 2006). The SAM can dramatically affect the sea–ice–air coupled system, and may couple with other climate modes, thereby exerting significant influence on global climate (Zheng et al., 2014; Ma et al., 2016). The SAM may also act as a bridge between sudden stratospheric warming and the surface climate response (Baldwin et al., 2003; Shen et al., 2020; Jian et al., 2020).

The SAM has broad spectral characteristics in terms of time scale. Besides the intrinsic time scale of 10 days (Li and Li, 2009; Hartmann and Lo, 1998), the SAM can be detected at the monthly scale when its signal is continuous (Li and Li, 2012; Thompson and Wallace, 2000). Li and Wang (2003), Li and Li (2010), and Li (2015) stated that the SAM is mainly characterized by a zonally symmetric and equivalent barotropic structure—that is, two out-of-phase anomalous pressure belts spanning along a zonal circle from the surface to the upper troposphere in the middle (40°S) and high (60°S) latitudes of the Southern Hemisphere, respectively. The SAM's structure is basically consistent between the surface and the middle and upper troposphere. The zonal uniformity of the geography in the Southern Hemisphere reinforces the zonal symmetry

* Corresponding author.
E-mail address: lixiuzhen@mail.sysu.edu.cn (X. Li).

https://doi.org/10.1016/j.aosl.2022.100206
Received 1 November 2021; Revised 14 February 2022; Accepted 4 March 2022
Available online 10 March 2022

of the SAM's structure (Hall and Visbeck, 2002). However, a later study showed that some SAM events are characterized by a locally asymmetric structure, especially in its negative phase over the Pacific region in austral winter and spring, which explains as much as 25% of the total variability (Fogt et al., 2012). Fan (2007) also confirmed that the covariance of SAM indices in the western and eastern hemispheres is weak. The asymmetries of the SAM may result from the superposition of other circulation modes (e.g., the Pacific–South America pattern), the high terrain near South America, and seasonal effects (Lefebvre and Goosse, 2005; Zhang et al., 2018; Fogt et al., 2012; Yu et al., 2015).

Various zonal asymmetries in the SAM's structure can induce distinct climatic impacts. Fan (2007) demostrated that the zonal asymmetry of the SAM modulates the distribution of precipitation across the Southern Hemisphere in austral winter. Through model simulation, Marshall et al. (2011) noted that the variation in the non-annular component of the SAM (i.e., its zonally asymmetric structure) is the principal factor governing the regional relationship between the SAM and temperature. However, thus far, the underlying physical processes are not clearly understood (Li, 2015).

The SAM is also described as a "meridional vacillation of the polar jet" by considering its concurrence with the shift in the midlatitude zonal westerly (Thompson and Wallace, 2000; Lorenz and Hartmann, 2001; Fyfe and Lorenz, 2005). In turn, the maintenance of the SAM's structure is closely related to the interaction between the zonal mean flow and transient eddies around the polar front jet (PFJ) (Ding et al., 2012; Nie et al., 2013; Limpasuvan and Hartmann, 1999, 2000). Thus, one of the objectives of this study was to analyze the structure of the zonal westerly associated with different patterns of SAM events.

By considering different spatial structures of the SAM may induce different impacts, the aim of this study was to investiagte the asymmetric structure of the SAM and its relationship with the PFJ in the mid–high latitudes of the Southern Hemisphere. The rest of the paper is organized as follows: The data and methods used in this study are described in section 2. In section 3, the classfication of the patterns is presented. The diversity of different patterns with the PFJ in the mid–high latitudes is presented in section 4. Finally, a summary and some further discussion are given in section 5.

2. Data and methods

There are several methods of creating an index to monitor the spatiotemporal variability of the SAM (Ho et al., 2012; Fogt and Marshall, 2020). By referring to Gong and Wang (1999) and Fogt and Marshall (2020), the principal component of the first EOF mode extracted from the geopotential height over the Southern Hemisphere (20°S–90°S) is defined as the SAM index (SAMI). Three SAM indices—namely, $SAMI_{msl}$, $SAMI_{700}$, and $SAMI_{500}$—were obtained to represent the variation in the SAM at different levels (mean sea level, 700 hPa, and 500 hPa, respectively). To ensure the SAM signal was significant throughout the troposphere, only the months when the magnitudes of all three SAMIs were larger than 1 standard deviation were selected as SAM events for further study. There were 135 events selected during 1979–2019 for classification. To avoid the influence of terrain and consider the pressure in the free atmosphere (King and Turner, 1997), we used the 500-hPa geopotential height anomalies as the classification field.

In order to quantitatively describe the characteristics of the PFJ anomaly in each pattern of the SAM, a jet path detection method based on the zonal wind at 300 hPa within 30°S–65°S was applied (Gallego et al., 2005), and only the jet path in the range of 40°W–90°W is shown. ERA5 reanalysis data during 1979–2019 were applied in this study (C3S, 2017).

K-means cluster analysis (MacQueen, 1967) has for decades been a popular clustering method in the atmospheric and oceanic sciences (Johnson et al., 2013). The self-organizing map (SOM) (Kohonen, 2001)—an unsupervised type of artificial neural network—can extract nonlinear and asymmetric features in any spatiotemporally varying field, but it is a time-consuming method. As the SOM usually yields a relatively large number of classes, it was unsuitable in this study to use it by itself. In order to determine the K clusters precisely, two methods were combined to classify the patterns of SAM events according to Vesanto and Alhoniemi (2000), and all SOM–K-means calculations were performed with the Matlab SOM toolbox (http://www.cis.hut.fi/projects/somtoolbox/package/docs2/som_kmeans.html).

The cluster analysis was first applied to various values of K increasing from 2 to 20 in increments of 1. The number of statistically indistinguishable SOM cluster pairs as a function of K, according to the "false discovery rate" outcomes (e.g., Wilks, 2006; Johnson, 2013), was calculated (Fig. 1). As is shown, when the cluster number reached 9, indistinguishable cluster pairs of patterns appeared. Hence, the optimal cluster number was 8 in this study.

3. Different patterns of SAM events

Eight distinguishable patterns of SAM events resulting from SOM–K-means classification based on 500-hPa geopotential height anomalies are shown in Fig. 2, along with their occurrence frequency. They differed obviously in strength and spatial distribution and could be clustered into four groups according to the spatial distribution of the geopotential height anomaly center at high latitudes—that is, symmetric patterns (P1 and P5), split-center patterns (P2 and P6), West Antarctica patterns (P3, P4, and P7), and a tripole pattern (P8). In the symmetric patterns (P1/P5), a center of negative/positive geopotential height anomalies was distributed over the Antarctic continent south to 60°S, associated with a weaker out-of-phase anomaly spanning zonally in a belt in the midlatitudes. Such a relatively symmetric spatial distribution was the most salient feature that distinguished it from other patterns. The total occurrence frequency of these symmetric patterns was 23.8%. For the split-center patterns (P2/P6), the pressure anomaly center at high latitudes was not constrained over the Antarctic continent, but split into two parts with comparable intensity over East and West Antarctica. The occurrence frequencies of these patterns were lowest among the eight patterns (8.8% and 8.1% for the positive and negative phases, respectively). The West Antarctica patterns (P3/P7) were also characterized by split centers at high latitudes, but the signal over West Antarctica was much stronger than that over East Antarctica. The occurrence frequencies of these two patterns were highest, reaching as high as 16%/20%—double that of the split-center patterns. For P4, the spatial distribution of the geopotential height anomaly bore strong similarities to that of P3, with the strongest pressure anomaly center over West Antarctica in P4 shifting slightly eastwards from 120°W to 90°W and covering the Bellingshausen Sea. The occurrence frequencies of this pattern and the tripole pattern were comparable to those of the symmetric patterns. The tripole pattern (P8) exhibited a tripole structure at high latitudes, with three positive pressure anomaly centers extending towards three continents. Additionally, the pressure anomaly centers in the midlatitudes lay separately over the ocean instead of jointly in a belt, indicating a dominant zonal wavenumber 3 pattern (Zhang et al., 2018; Wachter et al., 2020).

4. The zonal westerly flow of different patterns of SAM events

Fig. 3 shows the configuration of zonal wind anomalies in different patterns. In the positive phase of the symmetric SAM pattern P1, enhanced westerly wind anomalies occurred near 60°S—the transition zone between high-latitude negative pressure anomalies and midlatitude positive pressure anomalies (Fig. 3(a)). Whereas, weakened westerly wind appeared in the midlatitudes near 40°S with a smaller magnitude. This indicates a poleward shift of the PFJ, consistent with the studies of Kidson and Sinclair (1995) and Codron (2007). It is important to note that the core of the intensified westerly wind was not distributed

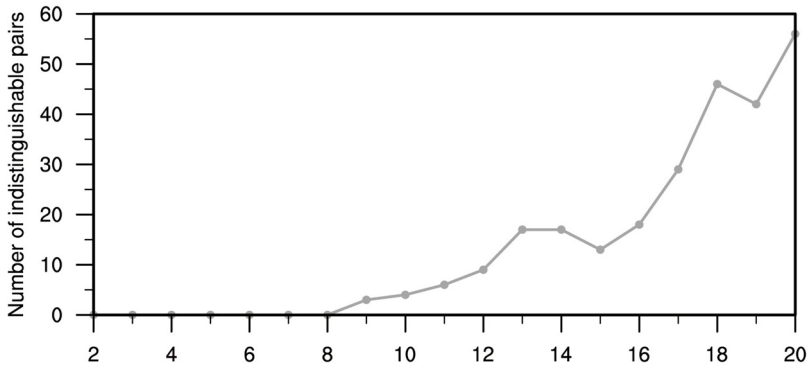

Fig. 1. The number of indistinguishable SAM pattern pairs clustered via the SOM method above the 95% confidence level. The horizontal axis indicates the number of patterns of SAM events (K) increasing from 2 to 20 in increments of 1.

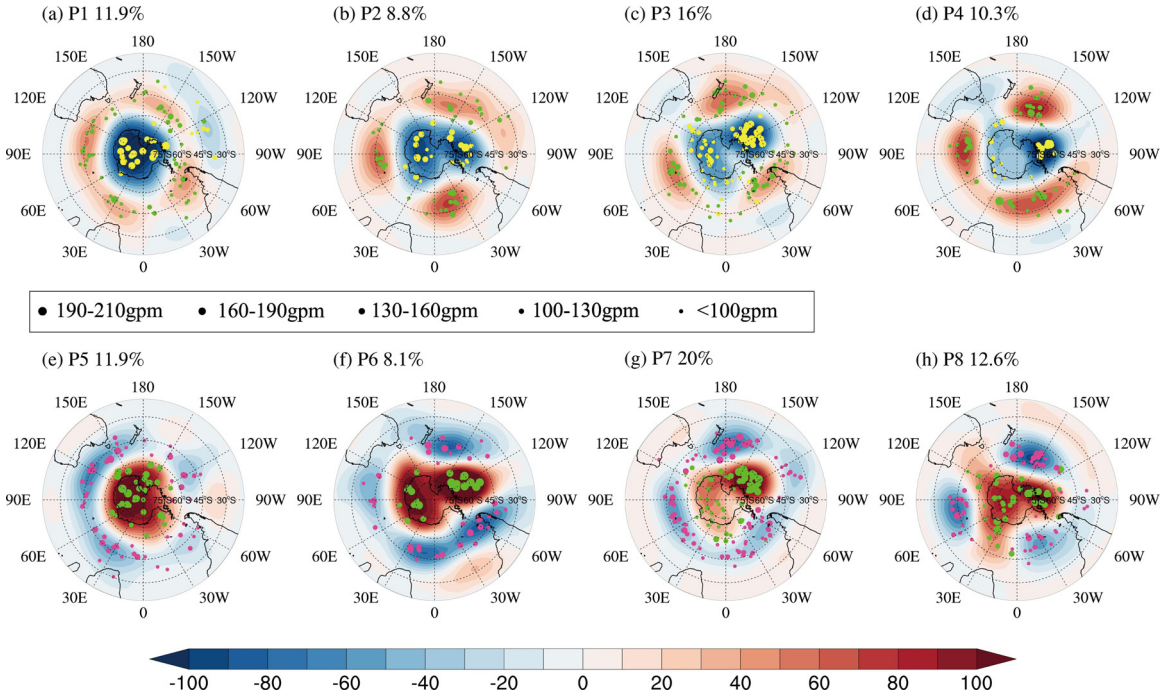

Fig. 2. Composite maps of geopotential height anomalies at 500 hPa based on (a–d) patterns of positive SAM events (P1–P4) and (e–f) patterns of negative SAM events (P5–P8) (shading; units: gpm; regions exceeding ±30 gpm are significant above the 95% confidence level). The occurrence frequency of each pattern is included in the top-left corner of each panel. The position and magnitude of each anomalous center in all cluster events are marked by dots.

in a zonally uniform manner; rather, it was skewed towards the Eastern Hemisphere near 120°E, south to Australia, nearly at the climatological exit of the PFJ. As a result, the PFJ not only shifted polewards, but also extended eastwards. The situation was nearly the opposite for the negative phase of the symmetric SAM pattern, with the PFJ shifting equatorwards, while the exit of the PFJ was nearly unchanged as the intensified westerly wind in the midlatitudes was weaker.

In other patterns, as the anomalous pressure accompanying the SAM was asymmetric, the adjusted zonally wind anomalies were more localized, instead of being distributed in a zonally uniform manner. The entrance and exit of the PFJ showed an obvious westward/eastward shift and diverse results were found in different patterns (Fig. 3(b–d), 3(f–h)). For example, in P3 and P7, where the split center over West Antarctica was much stronger than that over East Antarctica, the exit moved eastwards, while the entrance retreated eastwards in P3 and westwards in P7, illustrating an eastward shift of the whole PFJ in P3 and an extension of the whole PFJ both westwards and eastwards in P7, respectively.

To disclose the behavior of the PFJ more quantitatively, its meridional displacement and intensity were evaluated by detecting the jet path (Fig. 4). A poleward/equatorward shift tendency can be observed in all patterns of positive/negative SAM events, and it is more likely strengthened/weakened (Kidson and Sinclair, 1995; Thompson and Wallace, 2000). For the patterns of positive SAM events, the poleward displacement was largest near the entrance of the PFJ (around 40°W), as the enhanced midlatitude westerly tended to lay polewards and the climatological jet path was weak and situated more equatorwards in this region (Fig. 3(a–d)). The main body and the exit of the PFJ (0°–180°E) shifted polewards about 3°. Over the eastern Pacific Ocean (180°E–90°W) where the westerly wind was relatively weak (<30 m s^{-1}), the anomalous meridional displacement of the westerly jet was diverse in its patterns of symmetry. The poleward movement of the PFJ in P1 was the strongest because the anomalous pressure gradient was larger and situated more polewards than for other patterns. In contrast, the PFJ in P2/P3 was displaced equatorwards in 110°–90°W, which may have resulted from the equatorward shift of the split center at high latitudes over West Antarctica (Fig. 2(b, c)). In terms of the strength of the PFJ, this was weakened slightly near the entrance, whereas it was intensified over the main body and the exit for the patterns of positive SAM events. The wind speed increased dramatically over the South Pacific Ocean (reaching as high as 38.4% stronger than its normal state; Fig. 4(c)). This

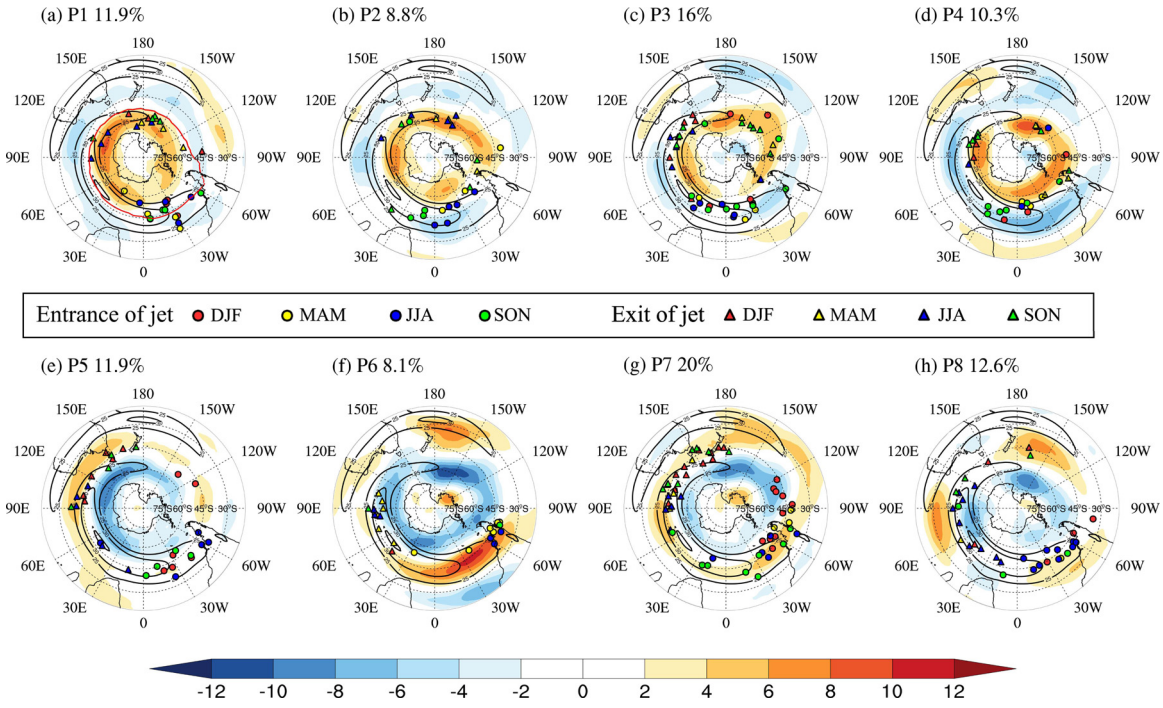

Fig. 3. Climatological zonal wind at 300 hPa (contours; units: m s^{-1}) and composites of monthly zonal wind anomalies for (a–d) patterns of positive SAM events (P1–P4) and (e–f) patterns of negative SAM events (P5–P8) (shading; units: m s^{-1}; significant above the 95% confidence level). The entrance (dots) and exit (triangles) of the westerly jet (≥ 30 m s^{-1}) in each season are marked in red, yellow, blue, and green for each event, separately. The climatological jet path (red line) is superimposed in (a).

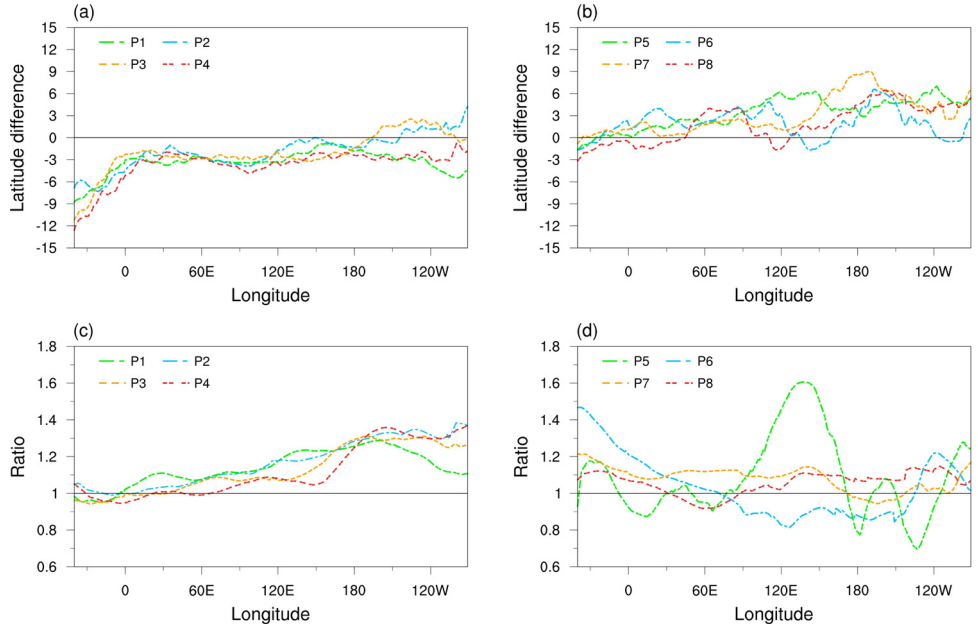

Fig. 4. (a, b) Composite meridional deviation of the jet path from the climatological displacement in patterns of (a) positive SAM events (P1–P4) and (b) negative SAM events (P5–P8) (units: °N). (c, d) Ratio of jet velocity to its climatology in patterns of (c) positive SAM events (P1–P4) and (d) negative SAM events (P5–P8).

could be further verified by the eastward shift of the jet exit (Fig. 3(a–d)). Within the four patterns of positive SAM events, the intensification of the westerly jet over the South Pacific was larger in three asymmetric patterns, which was closely related to the split high-latitude centers towards lower latitudes near West Antarctica.

For the patterns of negative SAM events, the westerly flow shifted equatorwards by about 4° in general. However, diversity was found within four patterns, and the zonal discrepancy was large within each negative SAM pattern—especially the asymmetric patterns (Fig. 4(b))—that is, the change in westerly flow was more localized in the patterns of negative SAM events. Similar characteristics were found in the strength of the PFJ (Fig. 4(d)). The westerly flow shifted equatorwards, south to Australia, near the exit of the PFJ, and intensified by up to 60% in the symmetric pattern (P5), whereas the variations in wind speed in the asymmetric patterns were much weaker, as the PFJ showed a larger meridional component. Hence, the spatial pattern of

the SAM could dramatically affect the displacement and intensity of the PFJ, and different PFJ variations could be found in the symmetric and asymmetric patterns.

5. Summary and discussion

Eight different patterns of SAM events in the Southern Hemisphere were identified by using SOM analysis in this study, among which two patterns (P1 and P5) represented a symmetric structure, whereas the other patterns showed considerable zonal asymmetry. In general, the zonal westerly flow moves polewards/equatorwards and enhances/weakens in positive/negative patterns, especially over the Pacific. Different PFJ variations in terms of meridional displacement and strength were found in different patterns. The more asymmetric the spatial distribution of the SAM, the more localized the adjusted zonally wind anomaly. In some asymmetric structures, as the adjusted wind field is characterized by a large meridional displacement, it might be likely that the PFJ will weaken. In addition, the entrance and exit of the jet change in most of the patterns, especially in the asymmetric patterns, which implies different climate impacts of the SAM. In this work, we explored concrete asymmetric patterns of the SAM, which vary in structure and the meridional movement of the PFJ—something that has not been specifically discussed in previous studies. This may help towards better understanding the different responses of the climate to the SAM pattern in certain key regions.

In this study, the SAM events in each month were considered with the annual cycle removed during data processing. However, the selected SAM events and the cluster patterns still showed some seasonal tendencies (Fig. S1 and Fig. S2; Fogt et al., 2012; Cordon, 2005, 2007), as well as a meridional displacement of the climatological PFJ (Barnes and Hartmann, 2010). Generally, the meridional displacements of the jet entrance and exit in different patterns did not show a strong seasonal dependence (Fig. 3). For example, P1 did not show an obvious difference (Fig. 3(a)), but in Fig. 3(g), the entrances in December–January–February shift significantly more to the west than those in September–October–November. Hence, it would be interesting in future work to study the seasonal variation tendencies of different patterns and their impact on the PFJ and climate.

In this study, the newly released ERA5 reanalysis data were applied to study the SAM and PFJ. Although numerous improvements and advances have been found in ERA5 (Hersbach et al., 2020), limitations of reanalysis data, such as the relatively poorer quality in the Southern Hemisphere as a result of the smaller availability of station-based observations, still need to be considered. In fact, an intercomparison of the geopotential height in the Southern Hemisphere between different reanalysis data and TOVS satellite data was executed, revealing that different reanalysis data produce different magnitudes of geopotential height over the Antarctic—especially over high terrain (figure not shown). However, their temporal variances show a high degree of consistency. ERA5 was selected in this study by virtue of the fact that it is a new-generation reanalysis dataset comprising full coverage of current observing systems and with improved confidence in the data over the Southern Hemisphere (Hersbach et al., 2019).

Funding

This work was jointly supported by the National Natural Science Foundation of China [grant numbers 42088101 and 42175019] and Guangdong Province Key Laboratory for Climate Change and Natural Disaster Studies [grant number 2020B1212060025].

Supplementary materials

Supplementary material associated with this article can be found, in the online version, at doi:10.1016/j.aosl.2022.100206.

References

Baldwin, M.P., Stephenson, D.B., Thompson, D.W.J., Dunkerton, T.J., Charlton, A.J., O'Neill, A., 2003. Stratospheric memory and skill of extended-range weather forecasts. Science 301 (5633), 636–640. doi:10.1126/science.1087143.

Barnes, E.A., Hartmann, D.L., 2010. Dynamical feedbacks of the Southern Annular Mode in winter and summer. J. Atmos. Sci. 67 (7), 2320–2330. doi:10.1175/2010JAS3385.1.

Codron, F., 2005. Relations between annular modes and the mean state: Southern hemisphere summer. J. Clim. 18, 320–330. doi:10.1175/JCLI-3255.1.

Codron, F., 2007. Relations between Annular Modes and the mean state: Southern hemisphere winter. J. Atmos. Sci. 64 (9), 3328–3339. doi:10.1175/JAS4012.1.

C3S (Copernicus Climate Change Service), 2017. ERA5: Fifth generation of ECMWF atmospheric reanalyses of the global climate. Copernicus Clim. Change Serv. Clim. Data Store (CDS) 20 (10), 2020. https://cds.climate.copernicus.eu/cdsapp#!/home.

Ding, Q., Steig, E.J., Battisti, D.S., Wallace, J.M., 2012. Influence of the tropics on the Southern Annular Mode. J. Clim. 25 (18), 6330–6348. doi:10.1175/JCLI-D-11-00523.1.

Fan, K., 2007. Zonal asymmetry of the Antarctic Oscillation. Geophys. Res. Lett. 34, L02706. doi:10.1029/2006GL028045.

Fogt, R.L., Jones, J.M., Renwick, J., 2012. Seasonal zonal asymmetries in the Southern Annular Mode and their impact on regional temperature anomalies. J. Clim. 25 (18), 6253–6270. doi:10.1175/JCLI-D-11-00474.1.

Fogt, R.L., Marshall, G.J., 2020. The Southern Annular Mode: Variability, trends, and climate impacts across the Southern Hemisphere. WIREs Clim. Change 11, e652. doi:10.1002/wcc.652.

Fyfe, J.C., Lorenz, D.J., 2005. Characterizing midlatitude jet variability: Lessons from a simple GCM. J. Clim. 18 (16), 3400–3404. doi:10.1175/JCLI3486.1.

Gallego, D., Ribera, P., Garcia-Herrera, R., Hernandez, E., Gimeno, L., 2005. A new look for the Southern Hemisphere jet stream. Clim. Dyn. 24, 607–621. doi:10.1007/s00382-005-0006-7.

Gillett, N.P., Kell, T.D., Jones, P.D., 2006. Regional climate impacts of the Southern Annular Mode. Geophys. Res. Lett. 33, L23704. doi:10.1029/2006GL027721.

Gong, D., Wang, S., 1999. Definition of Antarctic Oscillation index. Geophys. Res. Lett. 26, 459–462. doi:10.1029/1999GL900003.

Hall, A., Visbeck, M., 2002. Synchronous variability in the southern hemisphere atmosphere, sea ice, and ocean resulting from the Annular Mode. J. Clim. 15 (21), 3043–3057. doi:10.1175/1520-0442(2002)015<3043:SVITSH>2.0.CO;2.

Hersbach, H., Bell, B., Berrisford, P., Horányi, A., Joaquín, M-S., Nicolas, J., Radu, R., et al., 2019. Global Reanalysis: Goodbye ERA-Interim, Hello ERA5. ECMWF Newsletter No. 159. Spring, pp. 17–24. doi:10.21957/vf291hehd7.

Hersbach, H., Bell, B., Berrisford, P., Hirahara, S., Horányi, A., Joaquín, M-S., Nicolas, J., et al., 2020. The ERA5 global reanalysis. Q. J. R. Meteorol. Soc. 146, 1999–2049. doi:10.1002/qj.3803.

Hartmann, D.L., Lo, F., 1998. Wave-driven zonal flow vacillation in the Southern Hemisphere. J. Atmos. Sci. 55 (8), 1303–1315. doi:10.1175/1520-0469(1998)055<1303:WDZFVI>2.0.CO;2.

Ho, M., Kiem, S., Verdon-Kidd, D.C., 2012. The Southern Annular Mode: a comparison of indices. Hydrol. Earth Syst. Sci. 16, 967–982. doi:10.5194/hess-16-967-2012.

Jian, R., Garfinkel, C.I., White, I.P., Schwartz, C., 2020. The Southern Hemisphere minor sudden stratospheric warming in September 2019 and its predictions in S2S models. J. Geophys. Res. Atmos. 125, e2020JD032723. doi:10.1029/2020JD032723.

Johnson, N.C., 2013. How many ENSO flavors can we distinguish? J. Clim. 26 (13), 4816–4827. doi:10.1175/JCLI-D-12-00649.1.

Kidson, J.W., Sinclair, M.R., 1995. The influence of persistent anomalies on southern hemisphere storm tracks. J. Clim. 8 (8), 1938–1950. doi:10.1175/1520-0442(1995)008<1938:TIOPAO>2.0.CO;2.

King, J.C., Turner, J., 1997. Antarctic Meteorology and Climatology. Cambridge University Press, New York.

Kohonen, T., 2001. Self-Organizing Maps, third ed. Springer-Verlag, New York.

Lefebvre, W., Goosse, H., 2005. Influence of the Southern Annular Mode on the sea ice-ocean system: The role of the thermal and mechanical forcing. Ocean Sci. 1, 145–157. doi:10.5194/os-1-145-2005.

Li, J., Wang, J.X.L., 2003. A modified zonal index and its physical sense. Geophys. Res. Lett. 30, 1632. doi:10.1029/2003GL017441.

Li, X., Li, J., 2009. Main submonthly timescales of northern and southern hemispheres annual modes. Chin. J. Atmos. Sci. 33 (2), 215–231. doi:10.3878/j.issn.1006-9895.2009.02.02.

Li, X., Li, J., 2010. Propagation characteristics of atmospheric circulation anomalies of sub-monthly Southern Hemisphere annular mode. Chin. J. Atmos. Sci. 34 (6), 1099–1113. doi:10.3878/j.issn.1006-9895.2010.06.06.

Li, X., Li, J., 2012. Analysis of the quasi-geostrophic adjustment process of the Southern Hemisphere annular mode. Chin. J. Atmos. Sci. 36 (4). doi:10.3878/j.issn.1006-9895.2012.11142.

Li, X., 2015. Review of the introduction and debates of the Annular Modes. Adv. Atmos. Sci. 30 (3), 367–384. doi:10.11867/j.issn.1001-8166.2015.03.0367.

Limpasuvan, V., Hartmann, D.L., 1999. Eddies and the annular modes of climate variability. Geophys. Res. Lett. 26 (20), 3133–3136. doi:10.1029/1999GL010478.

Limpasuvan, V., Hartmann, D.L., 2000. Wave-maintained Annular Modes of climate variability. J. Clim. 13, 4414–4429. doi:10.1175/1520-0442(2000)013<4414:WMAMOC>2.0.CO;2.

Lorenz, V., Hartmann, D.L., 2001. Eddy-zonal feedback in the Southern Hemisphere. J. Atmos. Sci. 58, 3312–3327. doi:10.1175/1520-0469(2001)058<3312:EZFFIT>2.0.CO;2.

Ma, H., Li, Z., Zhang, L., 2016. Review on the impacts of the southern annular mode on climate over China. Plateau Meteorol. 35 (6), 1595–1608. doi:10.7522/j.issn.1000-0534.2015.00098.

MacQueen, J., 1967. Some methods for classification and analysis of multivariate observations. In: Proc. Fifth Berkeley Symposium on Mathematical Statistics and Probability, Statistics, I. University of California Press, Berkeley, pp. 281–297.

Marshall, G.J., Di Battista„ S., Naik, S.S., Thamban, M., 2011. Analysis of a regional change in the sign of the SAM–temperature relationship in Antarctica. Clim. Dyn. 36, 277–287. doi:10.1007/s00382-009-0682-9.

Nie, Y., Zhang, Y., Yang, X.Q., Chen, G., 2013. Baroclinic anomalies associated with the Southern Hemisphere Annular Mode: Roles of synoptic and low-frequency eddies. Geophys. Res. Lett. 40, 2361–2366. doi:10.1002/grl.50396.

Shen, X., Wang, L., Osprey, S., 2020. Tropospheric forcing of the 2019 Antarctic sudden stratospheric warming. Geophys 47, e2020GL089343. doi:10.1029/2020GL089343.

Thompson, D.W.J., Wallace, J.M., 2000. Annular modes in the extratropical circulation. Part I: month-to-month variability. J. Clim. 13 (5), 1000–1016. doi:10.1175/1520-0442(2000)013<1000:AMITEC>2.0.CO;2.

Vesanto, J., Alhoniemi, E., 2000. Clustering of the self-organizing map. IEEE Trans. Neural Netw. 11 (3), 586–600. doi:10.1109/72.846731.

Wachter, P., Beck, C., Philipp, A., Höppner, K., Jacobeit, J., 2020. Spatiotemporal variability of the Southern Annular Mode and its influence on Antarctic surface temperatures. J. Geophys. Res. Atmos. 125, e2020JD033818. doi:10.1029/2020JD033818.

Wilks, D.S., 2006. On “field significance” and the false discovery rate. J. Appl. Meteorol. Climatol. 45 (9), 1181–1189. doi:10.1175/JAM2404.1.

Yu, J., Paek, H., Saltzman, E.S., Lee, T., 2015. The early 1990s change in ENSO–PSA–SAM relationships and its impact on southern hemisphere climate. J. Clim. 28 (23), 9393–9408. doi:10.1175/JCLI-D-15-0335.1.

Zhang, Z., Uotila, P., Stössel, A., Vihma, T., Liu, H., Zhong, Y., 2018. Seasonal southern hemisphere multi-variable reflection of the southern annular mode in atmosphere and ocean reanalyses. Clim. Dyn. 50, 1451–1470. doi:10.1007/s00382-017-3698-6.

Zheng, F., Li, J., Liu, T., 2014. Some advances in studies of the climatic impacts of the Southern Hemisphere annular mode. Acta Meteorol. 72 (5), 926–939. doi:10.1007/s13351-014-4079-2.